Electric Control on the Nanoscale Using Tubular Image States

Dvira Segal,[a] Petr Král,[b] and Moshe Shapiro[c,d,*]
[a]Department of Chemistry, Columbia University, 3000 Broadway, New York, New York 10027, USA
[b]Department of Chemistry, University of Illinois at Chicago, Chicago, Illinois 60607, USA
[c]Department of Chemical Physics, Weizmann Institute of Science, Rehovot 76100, Israel
[d]Department of Chemistry, University of British Columbia, Vancouver V6T 1Z1, Canada

(Received 13 November 2006)

Abstract. We discuss the use of Tubular Image States (TIS) of electrons in the vicinity of nanotubes as a new vehicle for controlling and optically addressing nanoscale devices. We show that the stability of the TIS arises from the interplay between the attractive image potentials and the repulsive centrifugal potentials arising from the rotation of the electron about the cylindrically shaped nanotubes. We discuss the theory and some of the potential applications of TIS, and, in particular, the trapping of a single electron by a quadrupole made up of four nanotubes in the so-called "nano-Paul trap" configuration.

1. INTRODUCTION

Image potential states (IPS) are excited states of electrons that exist in the vicinity of surfaces. They resemble many of the properties of atomic and molecular Rydberg states.[1] IPS result from the attractive potential between an electron outside the surface of a conducting solid and its electrostatic image. When the penetration of the electronic states inside the bulk is prohibited, the image states form a quantized energy set converging towards the vacuum level.

When an electron exists at a distance z above a *flat* conductor, the attractive image potential given as $Vz = -e^2/4z$ is identical to the potential produced by a positive (mirror) charge at a distance z inside the material. Because of the $1/z$ attraction, the image potential can support a series of Rydberg-like states whose energies, given as $E_n = -0.85eV/(n + a)^2$, where $n = 1,2,3$, is the principal quantum number, converge as $n \rightarrow \infty$ to the "vacuum energy".

Höfer et al.[2] have used two-photon photoemission to populate and probe coherent wave packets of image states above a Cu(100) surface. In this experiment one photon excites an electron out of an occupied state below the Fermi energy into an image potential state. A second photon excites the electron to an energy above the vacuum level. By varying the photon energy and detecting the electronic energy, one can obtain "images" of these states.

In flat-surfaced metals, the lifetimes of image states is limited to a few picoseconds due to the annihilation of the electrons on the surface. These lifetimes scale with n as $\tau_n = n^3$, due to the reduction in overlap of the high n electrons with the surface. Similar experiments performed above molecular wires laid on surfaces,[3] nanoparticles,[4] and one- and two-dimensional liquid helium[5] demonstrated that extended image states are common in nanoscale systems. However, practical applications of image states above flat metallic surfaces are limited by their short lifetimes.[6]

Recently, a new class of electronic image states existing in the vicinity of cylindrically shaped objects, such as metallic nanotubes, called "Tubular Image States", were predicted to exist.[7] These states ought to be much more stable than image states above flat surfaces, due to the interplay between the attractive image potential and the repulsive centrifugal potential associated with their

*Author to whom correspondence should be addressed.
E-mail: mshapiro@chem.ubc.ca

non-zero angular momentum l. The "centrifugal barrier" thus formed prohibits the electron from reaching the surface and being annihilated there, while the attractive image potential prevents the electron from escaping the nanotube region.

TIS in finite-sized systems can also be longitudinally localized along the nanowire main axis by designed inhomogeneities,[8] and can be tuned by external electric and magnetic fields.[9] In addition, *bands* of TIS can be formed above 1D and 2D periodic arrays of nanotubes.[10] The collapse of these states on the material surface is predicted to be very slow and to be mainly due to the excitation of circularly polarized phonons.[11] TIS are also an interesting and rich platform for investigating quantum chaos in the nanoscale.[12]

The existence of IPS with *prolonged lifetime* was recently confirmed in multiwalled nanotubes. Similarly to the flat metal experiment,[2] in this case also the image states were populated by a two-photon photoemission, where one photon photoexcites an electron out of an occupied state below the Fermi level into an image potential state, and a second photon promotes this image electron to an energy above the vacuum level. The resulting kinetic energy provides information on the image states binding energies and lifetimes,[13] which nicely agree with the theoretical predictions.[14] It is expected that similar states could be observed around single-wall nanotubes and nanotube bundles.

2. THEORY

Following ref 7, we consider a charge q_0 placed at a distance ρ relative to the center of a perfectly conducting, infinitely long tube of radius a. The potential of interaction between the charge and the charges it induces on the metallic surface can be shown to be asymptotically equal to

$$V(\rho) \sim \frac{-q_0^2}{a} \frac{1}{\rho \ln(\rho/a)} \qquad (1)$$

The effective interaction potential $V_{eff}(\rho)$, shown in Fig. 1, is formed by adding to the attractive induced potential the repulsive centrifugal potential

$$V_{eff}(\rho) = V(\rho) + \frac{\hbar^2\left(l^2 - 1/4\right)}{2m_e\rho^2} \qquad (2)$$

where m_e is the electron mass.

For moderate angular momenta ($l \geq 6$), the effective potential possesses extremely long-range wells that can support bound TIS. The high centrifugal barrier prevents the electron from collapsing onto the surface. The wave functions associated with the TIS-electron motion in this potential are separable in the cylindrical coordinate. Assuming that the potential along the longitudinal z direction is homogeneous, we have

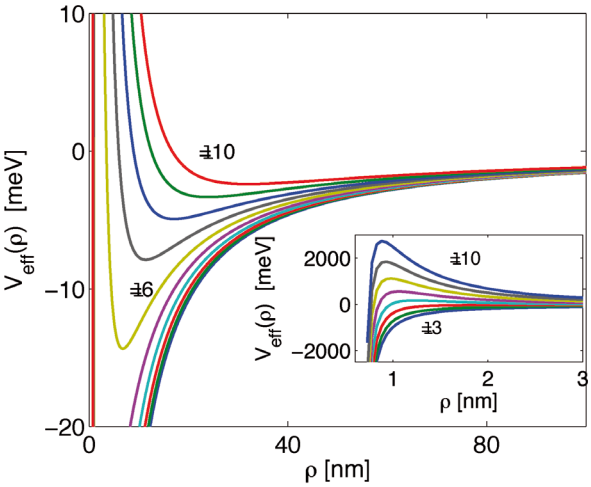

Fig. 1. The effective potential between an electron and a conducting nanotube shown for a number of angular momenta l, and a = 0.68 nm. Long-range minima are seen for $l > 6$. The inset shows a blowup of the potential near the surface of the nanotube where a large potential barrier exists.

$$\Psi_{n,l,k}(\rho,\phi,z) = \psi_{n,l}(\rho)\exp(il\phi)\phi_k(z)/\sqrt{2\pi\rho} \qquad (3)$$

The variation of these wave functions with n is depicted in Fig. 2. The corresponding eigenenergies are $E_{n,l,k} = E_{n,l} + E_k$, where $E_{n,l}$ is related to the radial electronic motion, and E_k is the energy for the longitudinal motion along the wire. The radial wave function $\psi_{n,l}(\rho)$ satisfies the Schrödinger equation

$$\left(-\frac{\hbar^2}{2m_e}\frac{d^2}{d\rho^2} + V_{eff}\left(\rho^2\right) - E_{n,l}\right)\psi_{n,l}(\rho) = 0 \qquad (4)$$

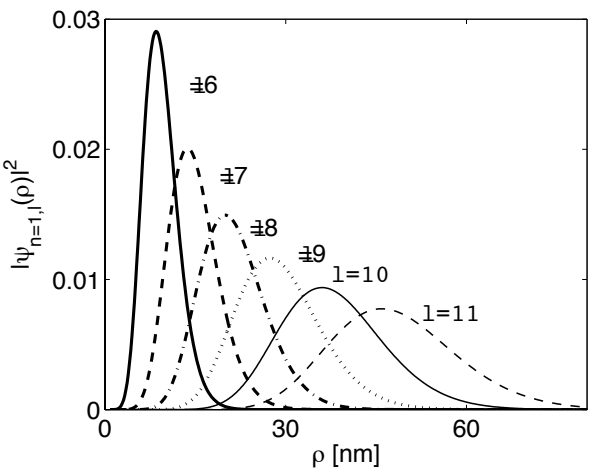

Fig. 2. The n = 1 wave functions (squared) for the set of potentials shown in Fig. 1.

The eigenstates corresponding to a few meV of binding energies are highly extended from the surface.

3. APPLICATION: NANOSCALE PAUL TRAPPING OF A SINGLE ELECTRON

We now apply the above formulation to the construction of a "nano-Paul trap".[15] The nano-Paul trap is made up of four parallel conducting nanorods, e.g., metallic carbon nanotubes (CNT), spaced symmetrically about a central axis. Application of a properly tuned ac field to the nanorods can lead to two-dimensional ("radial") confinement of a *single* electron at the trap center. Confinement along the third ("axial") direction can be attained by manipulating the structure of the tubes and/or the shapes of the end-caps. In addition to the size, the major differences between such a nano-trap and its macroscopic analog are that the electron must be treated as a quantum object and that its effect ("back reaction") on the trapping device cannot be ignored.

As shown in Fig. 3a, the typical dimensions of the proposed device are in the nanometric range: The distance between the tubes is $d \sim 100$ nm, each tube's radius is $a \sim 0.7$ nm, and the tube's length is $L \sim 200$ nm. These requirements are within present-day technology.[16] The proposed device has to operate at very high frequencies, 100 GHz–1 THz, which recent studies of the ac performance of CNT suggest are realizable.[17]

We have calculated numerically the image potential interaction energy $V_0(x,y,z)$, including the electrostatic interaction between the rods, using the method of ref 8. A contour plot of this potential using the typical dimensions given above is displayed in Fig. 3(b). The depth of the potential at the center point is ~ –0.5 meV, while near the surface of each tube it goes down to –250 meV. It can be shown that far from the tubes ends, $z \sim 100$ nm, the axial variation of the potential is weak in comparison to the radial gradient.[8] For sufficiently long tubes it is therefore permissible to neglect the axial dependence of the potential.

As shown in Fig. 3a, by connecting the four tubes to an external ac source, oscillating at frequency Ω, where tube no. 1 and its diagonal counterpart, tube no. 4, are charged by Q and tube no. 2 and diagonal counterpart, tube no. 3, by $-Q$, we form an oscillating quadrupole. We can calculate $V_T(x,y,z)$, the total interaction energy of a charged particle with the nano-quadrupole in the presence of image charges by using a simple extension of our numerical procedure.[8] The total potential, V_T, is a sum of two terms,

$$V_T(x,y,t) = V_0(x,y) + V_Q(x,y)\cos(\Omega t) \qquad (5)$$

where V_0 is the image potential and V_Q, the "charging" potential, is the additional potential resulting from the added ac quadrupolar charges. The charging potential

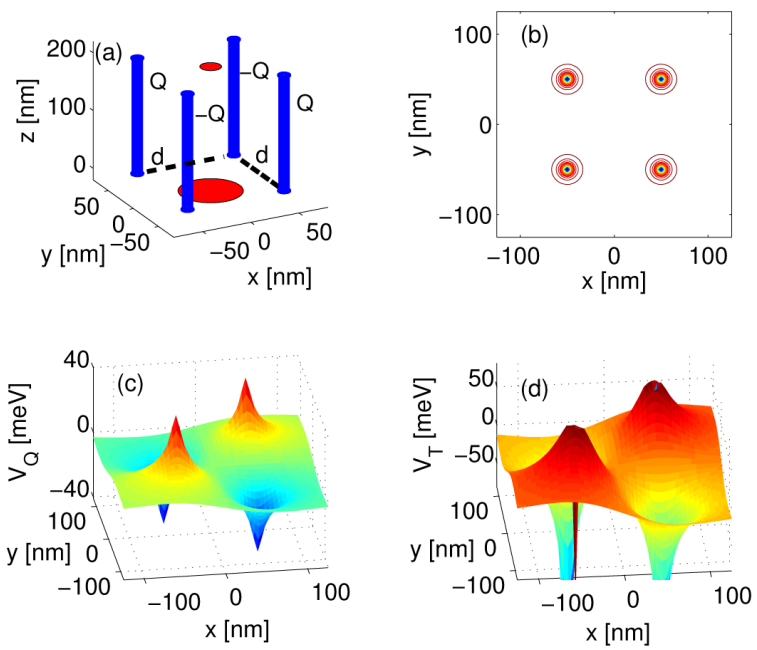

Fig. 3. (a) A schematic illustration of a nano-trap composed of four parallel tubes aligned in the z direction. The large circle represents the size of the incoming electronic wave packet and the small circle, the size of the trapped wave packet. (b) A contour plot of $V_0(x,y)$. (c) A surface plot of $V_Q(x,y)$, for $Q/L \equiv \lambda = 0.005$ e/nm. (d) The total potential energy function for $\lambda = 0.02$ e/nm. $z = 100$ nm in panels (b)–(d).

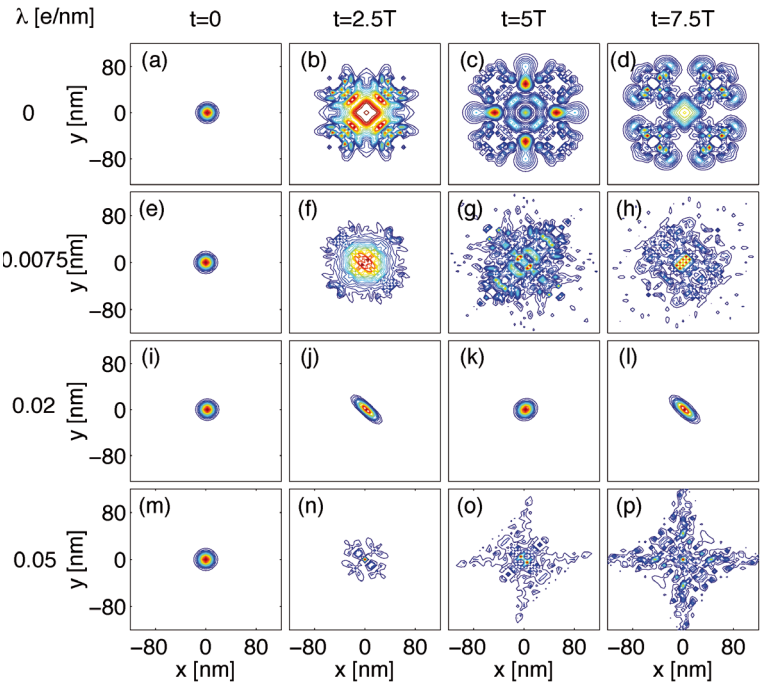

Fig. 4. Electron's probability-density for different charging potentials. (a)–(d) $\lambda = 0$; (e)–(h) $\lambda = 0.0075$ e/nm; (i)–(l) $\lambda = 0.02$ e/nm; (m)–(p) $\lambda = 0.05$ e/nm. The calculation is performed in an x–y 250 × 250 nm^2 lattice and for $\nu = 8.3\ 10^{11}$ Hz.

has an approximate quadrupolar spatial shape, as shown in Fig. 3c. Panel (d) presents the combination V_T that to a good approximation sustains the quadrupolar form.

As in conventional linear Paul traps[18] with ac charging, the saddle point at the center provides a point of stability where the electron can be confined.

The dynamics of a single electron subject to this potential is obtained by solving the time-dependent Schrödinger equation

$$i\hbar\partial_t\Psi(x,y,t) = \left[\frac{-\hbar^2}{2m_e}\left(\partial_x^2 + \partial_y^2\right) + V_T(x,y,t)\right]\Psi(x,y,t) \qquad (6)$$

where m_e is the electron mass. Unlike the case of a pure quadrupole,[18] and due to the presence of the image charge potential (V_0), this equation is non-separable in the x,y coordinates, and the analytical results of ref 19 cannot be applied. Given eq 6, the propagation of an initial wave packet can be computed using, e.g., the unitary split evolution operator propagation method.[20]

Due to the scaling properties of the Schrödinger equation,[6] it is possible to design traps of various spatial dimensions operating at different control conditions. Hence, the dynamics is invariant to the scaling up of the spatial and temporal coordinates $\alpha \rightarrow \sqrt{\kappa\alpha}$, $\Delta \rightarrow \kappa\Delta$, provided the frequency, charge density, and image potential are scaled down as

$$\Omega \rightarrow \Omega/\kappa, \quad \lambda \rightarrow \lambda/\kappa, \quad V_0 \rightarrow V_0/\kappa \qquad (7)$$

The scaling of the image potential, which roughly behaves as $1/[\rho\ln(\rho/a)]$, can be accomplished approximately by adjusting the tube's radii.

We are now in a position to demonstrate trapping and focusing of a single electron in the nano-trap. Figure 4 displays the time evolution of an initial (highly localized) Gaussian wave packet $\Psi(x,y,t=0) = \exp[-(x^2 + y^2)/2\sigma^2]/\sqrt{\kappa\sigma^2}$, of width $\sigma = 10.5$ nm, subject to different charging potentials and ac modulation frequency of $\nu \equiv 1/T \equiv \Omega/2\pi = 8.3\ 10^{11}$ Hz. The spatial parameters are as in Fig. 3. We see that the wave packet evolves into distinct shapes for different values of the applied potential: In the absence of the ac modulation the electron accumulates in the vicinity of the tubes, as shown in Fig. 4(a–d). For the case of weak charging potentials, shown in Fig. 4(e–h), the electron is neither trapped nor is it strongly attracted to the tubes. Rather, the wave packet slowly spreads while filling the entire inter-tube space. Tight focusing occurs when the charging is high enough in Fig. 4(i–l) with the wave packet oscillating in the middle of the trap between its original shape and an elliptical, yet highly focused, shape. When the charging becomes too high, confinement is lost, as shown in

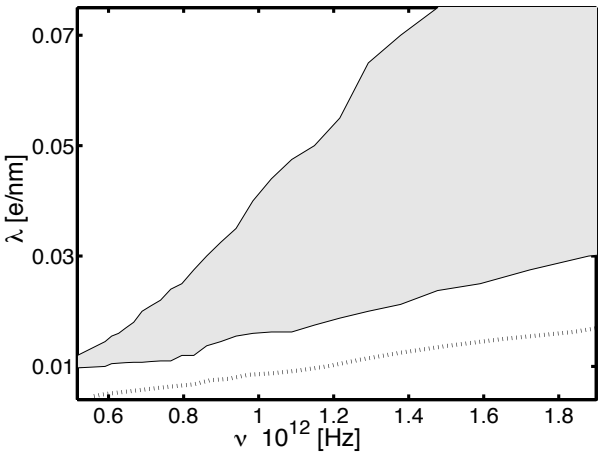

Fig. 5. A stability map of the nano-trap. Trapping exists in the shaded area. The dotted line marks the lower border of the stability region when the contribution of the image potential is removed from the Hamiltonian. This removal has no effect on the upper border line.

Fig. 4(m–p). The electron, though avoiding the tubes, manages to leak out by following the $x = 0$ and $y = 0$ lines. The wave packet evolution manifests the interplay between the image potential and the charging potential. In Fig. 4(a–d) the image potential dominates, leading to the collapse of the electron onto the nanotubes. In (e–h) the two potentials are of the same order, while in (i–p) the effect of the image potential is negligible.

A full characterization of the trap is presented in Fig. 5, where the stability diagram for different frequencies and charging potentials is provided. The diagram was generated by propagating for long times (~10 T) initially localized or unlocalized wave packets and recording whether at the end of the integration time the wave function remains confined at the trap center. We ascertained that the results are independent of the wave packet's initial shape. Note that due to the image potential, the range of stability is decreased. This effect ultimately limits the operation of very small traps to $d >$ 10 nm. Using eq 7 we can easily generate such diagrams for different spatial dimensions. The trap stability can also be studied as a function of an additional dc voltage, as is usually done in conventional Paul traps.[18]

Finally we note that an *axial* localization of the electron in the trap results naturally from the potential barriers imposed by the tube's end-caps.[8] This causes the electron to oscillate in both radial and axial directions at drastically different frequencies. Whereas the radial vibrational frequency is ~500 GHz, ν_z is ~ 10 GHz for the axial motion.[8] Strong axial confinement can be also achieved by applying a dc repulsive field on additional ring-shaped electrodes at the tube's ends.[18]

A single trapped electron is a promising candidate for a variety of quantum-information applications utilizing its spin states, the *anharmonic* quasienergy spectrum,[21] and its coupling to the nanowires mechanical modes.[22] Its dynamics can be manipulated either by magnetic fields or through coherent laser excitations. Of even greater interest would be *arrays* of electrons[23] trapped by a 2D lattice[10] of quartets of nano-traps of the type described here. Such arrays can be used as a set of entangled q-bits, where the degree of entanglement would be controlled by varying the ac charging, thereby allowing a greater or lesser portion of the electronic population to leak into neighboring cells and interact with other electrons confined there.

4. SUMMARY

Rydberg-like image states above nanostructures represent a new topic of interest with unique potential applications in optics, electronics, and surface science. Their manipulation by light fields can be utilized for quantum information storage and retrieval. Study of their localization properties and dynamics can provide important information about processes occurring on the nanotube surface. We have discussed the theoretical reasons for the TIS stability and their use in the creation of a nano-Paul trap. Our investigations can be easily generalized to include other nanorod structures that can now be fabricated, and to describe confinement of other charged particles besides electrons.

REFERENCES AND NOTES

(1) Gallagher, T. *Rydberg Atoms*; Cambridge University Press: New York, 1994.
(2) Höfer, U.; Shumay, I.L.; Reub, Ch.; Thomann, U.; Wallauer, W.; Fauster, Th. *Science* **1997**, *277*, 1480.
(3) Ortega, J.E.; Himpsel, F.J.; Haight, R.; Peale, D.R. *Phys. Rev. B* **1994**, *49*, 13859.
(4) Kasperovich, V.; Wong, K.; Tikhonov, G.; Kresin, V.V. *Phys. Rev. Lett.* **2000** *85*, 2729. Boyle, M.; Hoffman, K.; Schulz, C.P.; Hertel, I.V.; Levine, R.D.; Campbell, E.E. *Phys. Rev. Lett.* **2001**, *87*, 273401.
(5) Plazman, P.M.; Dykman, M.I. *Science* **1999**, *284*, 1967. Glasson, P.; Dotsenko, V.; Fozooni, P.; Lea, M.J.; Bailey, W.; Papageorgiou, G.; Andresen, S.E.; Kristensen, A. *Phys. Rev. Lett.* **2001**, *87*, 176802.
(6) Echenique, P.M.; Flores, F.; Sols, F. *Phys. Rev. Lett.* **1985**, *55*, 2348. Chulkov, E.V.; Sarria, I.; Silkin, V.M.; Pitarke, J.M.; Echenique, P.M. *Phys. Rev. Lett.* **1998**, *80*, 4947.
(7) Granger, B.E.; Král, P.; Sadeghpour, H.R.; Shapiro, M. *Phys. Rev. Lett.* **2002**, *89*, 135506.
(8) Segal, D.; Král, P.; Shapiro, M. *Phys. Rev. B* **2004**, *69*, 153405.
(9) Segal, D.; Král, P.; Shapiro, M. *Chem. Phys. Lett.* **2004**, *392*, 314.

(10) Segal, D.; Granger, B.E.; Sadeghpour, H.R.; Král, P.; Shapiro, M. *Phys. Rev. Lett.* **2005**, *94*, 016402.
(11) Segal, D.; Král, P.; Shapiro, M. *Surf. Sci.* **2005**, *577*, 86.
(12) Segal, D.; Král, P.; Shapiro, M. *J. Chem. Phys.* **2005**, *122*, 134705.
(13) Zamkov, M.; Woody, N.; Shan, B.; Chakraborty, H.S.; Chang, Z.; Thumm, U.; Richard, P. *Phys. Rev. Lett.* **2004**, *93*, 156803.
(14) Zamkov, M.; Chakraborty, H.S.; Habib, A.; Woody, N.; Thumm, U.; Richard, P. *Phys. Rev. B* **2004**, *70*, 115419.
(15) Segal, D.; Shapiro, M. *Nano Lett.* **2006**, *6*, 1622.
(16) Tu, Y.; Lin, Y.; Ren, Z.F. *Nano Lett.* **2003**, *3*, 107. Yu, Z.; Li, S.; Burke, P.J. *Chem. Mater.* **2004**, *16*, 3414.
(17) Burke, P.J. *Solid State Electron.* **2004**, *48*, 1981. Yu, Z.; Burke, P.J. *Nano Lett.* **2005**, *5*, 1403.
(18) Paul, W. *Rev. Mod. Phys.* **1990**, *62*, 531.
(19) Brown, L.S. *Phys. Rev. Lett.* **1991**, *66*, 527.
(20) Balakrishnan, N.; Kalyanaraman, C.; Sathyamurthy, N. *Phys. Rep.* **1997**, *280*, 79.
(21) Mancini, S.; Martins, A.M.; Tombesi, P. *Phys. Rev. A* **2000**, *61*, 012303.
(22) Tian, L.; Zoller, P. *Phys. Rev. Lett.* **2004**, *93*, 266403. Hensinger, W.K.; Utami, D.W.; Goan, H.-S.; Schwab, K.; Monroe, C.; Milburn, G.J. *Phys. Rev. A* **2005** *72*, 041405(R).
(23) Ciaramicoli, G.; Marzoli, I.; Tombesi, P. *Phys. Rev. Lett.* **2003**, *91*, 017901.